# Electronic and mechanical properties of planar and tubular boron structures

M. H. Evans,[1,2] J. D. Joannopoulos,[1] and S. T. Pantelides[2,3]
[1]*Department of Physics, Massachusetts Institute of Technology, Cambridge, Massachusetts 02139, USA*
[2]*Department of Physics and Astronomy, Vanderbilt University, Nashville, Tennessee 37235, USA*
[3]*Condensed Matter Sciences Division, Oak Ridge National Laboratory, Oak Ridge, Tennessee 37831, USA*
(Received 28 March 2005; revised manuscript received 26 May 2005; published 15 July 2005)

We report the results of first-principles calculations showing that boron can form a wide variety of metastable planar and tubular forms with unusual electronic and mechanical properties. The preferred planar structure is a buckled triangular lattice that breaks the threefold ground state degeneracy of the flat triangular plane. When the plane is rolled into a tube, the ground state degeneracy leads to a strong chirality dependence of the binding energy and elastic response, an unusual property that is not found in carbon nanotubes. The achiral $(n,0)$ tubes derive their structure from the flat triangular plane. The achiral $(n,n)$ boron nanotubes arise from the buckled plane, and have large cohesive energies and different structures as a result. $(n,n)$ boron nanotubes have an internal relaxation mechanism that results in a very low Poisson ratio. The strong variation in elastic properties of boron nanotubes makes them the mechanical analogue of carbon nanotubes, and may make them ideal candidates for applications in composite materials and nanoelectromechanical systems.

DOI: 10.1103/PhysRevB.72.045434 PACS number(s): 61.46.+w, 68.65.−k, 73.22.−f

Boron, carbon's first-row neighbor, has only three valence electrons. Its natural crystalline structure is a rhombohedral lattice with 12-atom icosahedral clusters at each lattice site.[1] Nevertheless, there are some intriguing similarities with carbon. Boron's three electrons could in principle form $sp^2$ hybrid orbitals that might lead to planar and tubular structures similar to those formed by carbon. Since carbon nanotubes and fullerenes[2] are metastable structures, formed only under kinetically constrained conditions,[3] one might envision analogous boron structures. Indeed, initial results by Boustani *et al.*[4,5] have demonstrated the possibility of such metastable structures with relatively low energy cost. Crystalline[6] and amorphous[7] boron nanowires with diameters as small as 20 nm have recently been fabricated, suggesting that boron nanotubes may already be within the range of experimental possibility.

There is an intriguing and potentially significant difference between carbon and boron, however. Boron has only three valence electrons, so that in $sp^2$-bonded planar or tubular boron structures the relative occupations of the $sp^2$- and the $\pi$-bonded bands depend on the energetic positions and dispersions of the two bands, perhaps opening up a broader range of possibilities.

In this paper, we examine in detail the electronic structure and relative stabilities of planar and tubular boron structures. We find that boron does form a stable $sp^2$-bonded hexagonal graphenelike sheet, but a planar triangular lattice has an even larger cohesive energy, though still smaller than that of the bulk $\alpha$-rhombohedral structure. The triangular planar structure has an unusual property. It is essentially a homogeneous electron gas system with a threefold-degenerate ground state. This degeneracy makes the flat triangular plane unstable with respect to buckling, which breaks the symmetry and introduces a preferred direction defined by $\sigma$ bonds. When rolled into a tube, this preferred direction, which is not present in carbon nanotubes, defines the chirality and controls the electron density, cohesive energy, and elastic response of boron nanotubes. The properties of the $(n,0)$ tubes (proposed in Refs. 4 and 5) arise from the flat plane and are very similar to carbon nanotubes. The properties of the $(n,n)$ boron nanotubes are derived from the buckled plane and contrast sharply with carbon nanotube structures. As a result of the buckling, the curvature energies of $(n,n)$ tubes are lower than those of $(n,0)$ tubes and show a nonmonotonic plateau structure as a function of $n$. The buckled sides of the larger $(4n,4n)$ boron nanotubes allow for internal relaxations that can dissipate longitudinal stress. As a result, larger $(4n,4n)$ tubes have a very low Poisson ratio. The resulting lateral rigidity is important for mechanical stress transfer in nanotube composite materials.[19]

The present calculations were based on the local density approximation (LDA) to Density Functional Theory,[8] a plane wave basis set,[9] and pseudopotentials[10] to represent the ionic cores. $K$-point meshes for Brillouin zone integration were sufficient to converge total energies to 1 mHa per atom. The boron pseudopotential accurately reproduces experimental[11] and theoretical[12] parameters for the $\alpha$-rhombohedral structure.

Figure 1(a) shows the in-plane electron density for the hexagonal plane. The structure, as would be expected by analogy to carbon, is $sp^2$-bonded, with high charge concentrations within the bond regions. However, the cohesive energy is only 5.96 eV, considerably lower than the 7.37 eV for the $\alpha$-rhombohedral phase. In both boron and carbon, the three $sp^2$ orbitals bind in the plane, forming bonding and antibonding states that are separated by a large energy gap. The $p$ orbitals perpendicular to the plane also bind weakly to each other (note that we are considering an isolated plane), forming bonding and antibonding bands that are degenerate at the K point in the Brillouin zone.[13] Carbon's four valence electrons fill all of the bonding bands from both the in-plane $sp^2$ orbitals and the $\pi$-bonded $p$ orbitals, resulting in a zero-gap semiconducting plane. In the hexagonal boron plane, the $\pi$-bonded band crosses the $sp^2$ bands, and there are not enough electrons to fill them all. The result is a metallic

 

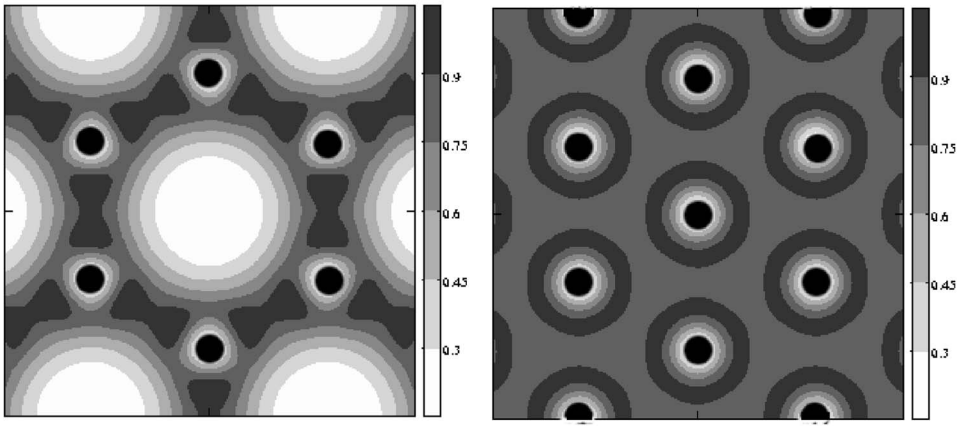


(a) The hexagonal boron plane. Note the $sp^2$ bonding, also found in graphite planes.

(b) The triangular boron plane. Outside of the ionic cores, the density is nearly uniform.

FIG. 1. Contour plot of the electron density for boron planes, in electrons/Å$^3$. The ionic cores are shown as black circles. Density fluctuations near the cores are characteristic of the pseudopotential. (a) The hexagonal boron plane. Note the $sp^2$ bonding, also found in graphite planes. (b) The triangular boron plane. Outside of the ionic cores, the density is nearly uniform.

plane without strong $sp^2$ binding, leading to a low cohesive energy.

Although the covalent hexagonal plane is not energetically favorable, the flat triangular plane has a cohesive energy of 6.53 eV, only 0.84 eV less than the $\alpha$-rhombohedral phase. The sharp contrast between this boron plane and graphite is striking. Figure 1(b) shows the in-plane electron density for the lowest energy flat triangular plane. The density is nearly uniform between the atoms, with little covalent character. Despite the nearly homogeneous electron density, the electronic bands are not free-electron-like. Figure 2 shows the boron bands and free electron bands from the $\Gamma$ point to the X point in the Brillouin zone. The free electron mass is scaled such that the free electron Fermi energy (with three electrons per primitive cell) is equal to the boron Fermi energy.

It is important to note that the sixfold coordination of the boron atoms in the triangular phase is not compatible with the symmetries of the $p$ orbitals (see Fig. 3). The best that can be hoped for is to let the $p_x$ orbital lie along a line of atoms, overlapping with the $p_x$ orbitals of two neighbors and forming $\sigma$ bonds. The $p_y$ orbital will have a much smaller overlap with the four remaining neighbors, forming mixed $\sigma$-$\pi$ bonds. This frustrated alignment of $p$ orbitals leaves the ground state indeterminate: three possible $\sigma$ bond directions can be chosen. In the flat triangular plane, symmetry makes these three directions equivalent, and the nearly homogenous electron density makes a metallic bonding picture more appropriate. However, the distinction between $\sigma$ and mixed $\sigma$-$\pi$ bonds has important consequences when the symmetry of the flat plane is broken.

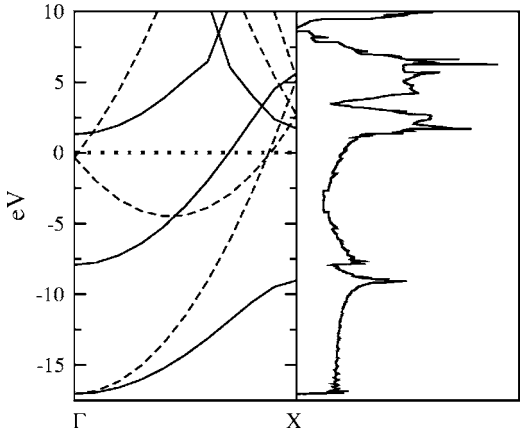


FIG. 2. Flat triangular lattice electronic bands for boron (solid) and free electrons (dashed), and boron density of states. The zero of energy is set at the Fermi energy.

A degenerate ground state suggests that the flat plane would be unstable with respect to buckling that breaks the triangular symmetry. This instability is confirmed by the phonon dispersion,[14] which has an acoustic branch with an imaginary frequency in the vicinity of the X point in the Brillouin zone. The imaginary frequency mode at the X point corresponds to the stable planar phase of boron, shown in Fig. 4(a). Instead of the nearly homogeneous electron density of the flat triangular plane, the buckled plane shows directional $\sigma$ bonds [see Fig. 4(b)], as would be expected from the $p$-orbital model presented above. In Fig. 4(b), the mixed $\sigma$-$\pi$ bonds do not contain enough electrons to appear on the isosurface. This buckled plane, which is distinct from the buckled boron sheet proposed in Ref. 5, selects a preferred direction and breaks the ground-state degeneracy, raising the cohesive energy to 6.79 eV. The high cohesive energy of the buckled plane suggests that the $\sigma$ bonds are strong, in the sense that a large amount of energy is required to break them.

The preferred bonding direction in the planar phase foreshadows the importance of chirality in nanotube phases. In

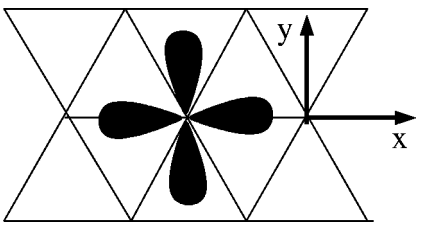


FIG. 3. $p_x$ and $p_y$ orbitals drawn schematically for a single atom on a triangular lattice (in the $x$-$y$ plane).

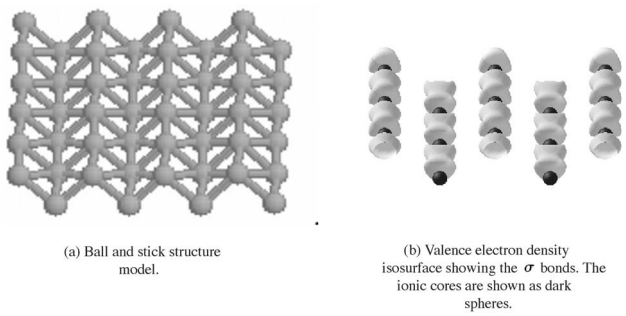


FIG. 4. The stable buckled triangular plane. (a) Ball and stick structure model. (b) Valence electron density isosurface showing the $\sigma$ bonds. The ionic cores are shown as dark spheres.

rolling up a triangular sheet to create a tube, the lines of $\sigma$ bonds can be chosen to run along the length of the tube, along its circumference, or to wind along it. The orientation of these bonds determines the electron density and energetics of the nanotube to an extent not seen in carbon nanotubes.[15] We define the chirality of a boron nanotube based on the triangular lattice. An $(m,n)$ tube is constructed by rolling a triangular plane such that the head of the lattice vector $m\vec{a}+n\vec{b}$ meets its tail; $\vec{a}$ and $\vec{b}$ are the primitive vectors of the triangular lattice.

Consider first the case of an $(n,n)$ nanotube, shown in Fig. 5. Here, the $\sigma$ bond direction can be chosen to lie along the length of the tube. Given this possibility, the boron atoms will form $\sigma$ bonds running along the nanotube, as the electron density isosurface in Fig. 5 shows. Instead of the circular cross section seen in carbon nanotubes, the (8,8) tube has a square cross section [shown in Fig. 6(b)]. The sides of the square are sections of the buckled plane, and the corners show only a slight distortion. In contrast, the cross section of the (6,6) tube [Fig. 6(a)] shows no buckling. With only four atoms on each side, it is not possible to buckle the sides without distorting the topology of the corners. The "buckled" structure of the (6,6) tube (Fig. 7) breaks the mirror symmetries of the actual (6,6) and (8,8) structures [Figs. 6(a) and 6(b)], introducing chirality to an achiral tube.

Larger diameter tubes sharing the favorable buckled structure of the (8,8) tube can be constructed by adding atoms to the sides of the square in pairs. Among the $(n,n)$ boron nanotubes, therefore, $(4n,4n)$ tubes should have lower curvature energies and be more stable. This trend is suggested by the

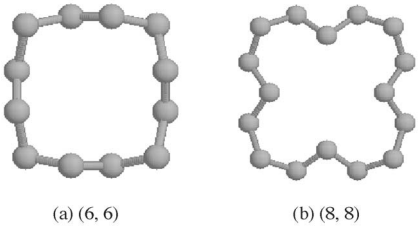


FIG. 6. Ball and stick cross sections of boron nanotubes.

cohesive and curvature energies summarized in Table I. In the table, the curvature energy is defined as the difference in cohesive energy between the tube and the plane: $E_{curv} \equiv E_{coh}^{tube} - E_{coh}^{plane}$.

An $(n,0)$ nanotube cannot align $\sigma$ bonds longitudinally (see Fig. 8). Although buckling and selecting a $\sigma$ bond direction proves energetically favorable in the $(n,n)$ tubes, it is not required by symmetry. Buckling is necessary to break the symmetry of the flat plane, but rolling up the plane into an achiral tube breaks the degeneracy automatically. The threefold planar degeneracy reduces to a twofold degeneracy (spiraling $\sigma$ bonds related by chiral symmetry) and a nondegenerate state ($\sigma$ bonds running longitudinally or laterally). It is possible for $\sigma$ bonds to run along the circumference of an $(n,0)$ tube, but the electron density of an (8,0) nanotube, shown in Fig. 8, shows no such bonds. Instead, the density of $(n,0)$ boron nanotubes is nearly uniform, exhibiting the free electron character of the flat triangular plane. Unlike the directional $\sigma$ bonds of the $(n,n)$ tubes, the $(n,0)$ tubes feature nondirectional metallic bonds. The $\sigma$ bonds of the $(n,n)$ boron nanotubes are similar to those of the buckled plane, while the metallic bonds of the $(n,0)$ tubes match those of the flat triangular plane. The curvature energies of $(n,0)$ boron nanotubes lie 0.25–0.4 eV above those of the $(n,n)$ tubes, roughly the same as the 0.26 eV cohesive energy difference between the flat and buckled triangular planes. Between the achiral limits, there may be a critical chiral angle at which boron nanotubes switch from the $\sigma$ bond dominated electronic structure of the buckled plane to the free-electron-like structure of the flat plane. This transition could have important consequences for the behavior of boron nanotubes under torsion.

Elastic properties of boron nanotubes exhibit a strong chirality dependence as well. Among the most important

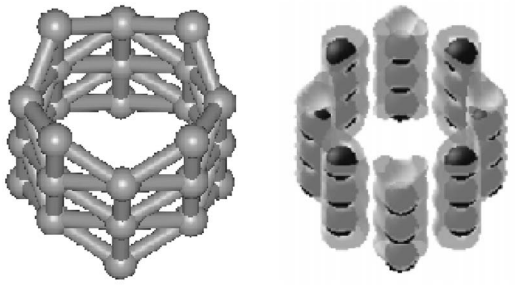

FIG. 5. The (4,4) boron nanotube. Left: ball and stick structure model. Right: valence electron density isosurface at 0.67 electrons/Å$^3$. The ionic cores are shown as dark spheres.

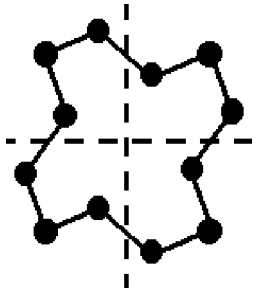

FIG. 7. Cross section of a proposed (6, 6) boron nanotube structure in which the sides buckle. The tube is not symmetric with respect to the mirror planes shown by dotted lines.

TABLE I. Summary of the cohesive energy $E_{coh}$, the curvature energy with respect to the buckled plane $E_{curv}$, the equilibrium diameter $d$, the modified Young's modulus $Y_s$ [see Eq. (1)], and the Poisson ratio $\sigma$ for boron nanotubes.

| Chirality | $E_{coh}$ (eV) | $E_{curv}$ (eV) | $d$ (Å) | $Y_s$ (TPA nm) | $\sigma$ |
|---|---|---|---|---|---|
| (4,4) | 6.71 | 0.08 | 4.34 | 0.29 | 0.5 |
| (6,6) | 6.65 | 0.14 | 5.65 | 0.15 | 0.4 |
| (8,8) | 6.76 | 0.03 | 8.48 | 0.22 | $<0.1$ |
| (7,0) | 6.36 | 0.43 | 3.99 | 0.49 | 0.2 |
| (8,0) | 6.39 | 0.40 | 4.62 | 0.49 | 0.1 |

characteristics of a cylindrical object is the Young's modulus $Y_s$, defined for single walled tubes as[15]

$$Y_s = \frac{1}{S_0}\left(\frac{\partial^2 E}{\partial \epsilon^2}\right)_{\epsilon=0}, \tag{1}$$

where $S_0$ is the equilibrium surface area, $E$ is the total energy, and $\epsilon$ is the longitudinal strain. Since the walls of our boron nanotubes are only a single atom thick, it is not possible to define the tube volume, and we must use this modified Young's modulus. For the $(n,n)$ tubes with square cross sections, we define the diameter as the diagonal of the square, and ignore buckling in calculating the surface area.

Another important elastic property of a tube is the Poisson ratio $\sigma$

$$\frac{d-d_{eq}}{d_{eq}} = -\sigma\epsilon, \tag{2}$$

where $d$ is the tube diameter at strain $\epsilon$, and $d_{eq}$ is the equilibrium tube diameter. The Poisson ratio measures the change in the tube's radius as it is strained longitudinally.

The calculated values for Young's moduli and Poisson ratios for various boron nanotubes are given in Table I, along with the corresponding cohesive energies. In order to understand the trends in the elastic constants and cohesive energies, we note the following. Cohesive energies are a measure of the depth of the effective potential well that produces binding (*strong* bonds correspond to deep wells). In contrast, the elastic constants are a measure of how steeply the effective potential rises from its minimum value (small second derivatives correspond to *soft* bonds, whereas large second derivatives correspond to *stiff* bonds).

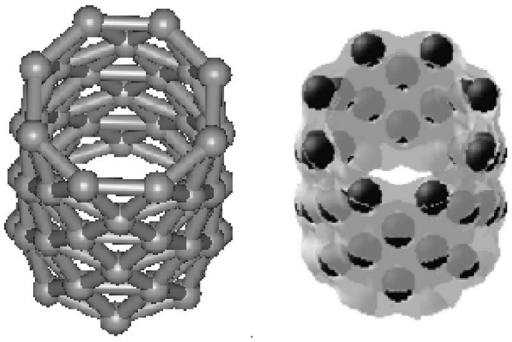

FIG. 8. The (8, 0) boron nanotube. Left: ball and stick structure model. Right: valence electron density isosurface at 0.67 electrons/Å$^3$. The ionic cores are shown as dark spheres.

According to Table I, the $(n,n)$ boron nanotubes have high cohesive energies in conjunction with relatively low Young's moduli. For example, the (4,4) tube has $Y_s = 0.29$ TPa nm, comparable to boron nitride nanotubes and roughly half that of carbon nanotubes.[15] This combination suggests that the longitudinal $\sigma$ bonds in the $(n,n)$ tubes are characterized by deep effective potential wells with a relatively small second derivative at the minimum. $\sigma$ bonds in $(n,n)$ boron nanotubes are strong, but soft. $(n,0)$ boron nanotubes, in contrast, have lower cohesive energies but higher Young's moduli. For the (8,0) tube, $Y_s = 0.49$ TPa nm. Although the radius of the (8,0) tube is only 6% larger than that of the (4,4) tube, the Young's modulus is 68% larger. This is in sharp contrast to carbon nanotubes, where tubes of similar radius have Young's moduli that differ by only a few percent.[15] The high Young's moduli of (8,0) boron nanotubes suggest that the nondirectional metallic bonds in these tubes are characterized by effective potential wells that are shallower than those of the $\sigma$ bonds, but have a larger second derivative at the minimum. Metallic bonds in $(n,0)$ boron nanotubes are weak [relative to the $\sigma$ bonds of the $(n,n)$ tubes] but stiff.

There are many examples in the literature of pairs of structures in which the stronger bonds are softer. A particularly relevant example is that of germanium and gray ($\alpha$) tin. Both Ge and $\alpha$-Sn share the diamond structure, but Ge is a direct gap semiconductor while $\alpha$-Sn is a semimetal. The cohesive energy of Ge is 3.85 eV/atom, while Sn is 3.14 eV/atom,[25] meaning that the bonds in Ge are stronger. However, the bulk modulus (equivalent to the Young's modulus for a bulk solid) for Ge is only 77 GPa, versus 111 GPa for Sn. Thus, although the Ge bonds are stronger, they are softer than those of Sn.

For the (4,4) tube, the Poisson ratio $\sigma = 0.5$, nearly twice as large as the value for either carbon or boron nitride nanotubes.[15] The high Poisson ratios of both the (4,4) and (6,6) boron nanotubes suggest that structural mechanisms may play a role in reducing the Young's modulus below what would be expected from the softness of the $\sigma$ bonds. A high Poisson ratio implies that the diameter of the tube changes significantly as the tube is strained longitudinally. The mixed $\sigma$-$\pi$ bonds along the circumference of the $(n,n)$ tubes allow the walls of the tube to relax and relieve the applied longitudinal stress. The strong relaxation of the tube walls, reflected in the Poisson ratio, reduces the energy cost to stretch the tube.

Structural dynamics play a more complex role in the (8,8) boron nanotube. Figure 6(b) shows that the cross section of the (8,8) tube is a square with buckled sides. Using the previous definition of the Poisson ratio, we find that $\sigma < 0.1$, considerably smaller than the Poisson ratio of the (4,4) and (6,6) tubes. The diameter of the (8,8) tube does not change significantly with strain, but there is considerable lateral relaxation that plays a role in lowering the Young's modulus. The simple square cross sections of the (4,4) and (6,6) tubes,

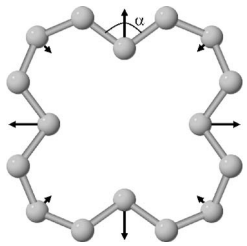


FIG. 9. Ball and stick cross section of the (8, 8) boron nanotube, with vectors showing lateral relaxations under positive longitudinal strain. Longer vectors represent larger relaxations, but are not to scale.

as well as the circular cross sections of the $(n,0)$ tubes, permit only uniform lateral dilation and contraction if the symmetry of the structure is to be maintained. The buckled sides of the (8,8) [and larger $(4n,4n)$ tubes, as discussed previously] permit tube walls to relax without changing the overall square structure. Figure 9 shows the lateral relaxations that the (8,8) tube undergoes under positive longitudinal strain.

Although the (8,8) boron nanotube does not change its diameter under longitudinal strain, the lateral mixed $\sigma$-$\pi$ bonds do allow for relaxation of the buckled tube sides. As the tube is stretched, the angle $\alpha$ in Fig. 9 increases. The increase in this buckling angle is also seen when the buckled plane is stretched along the lines of $\sigma$ bonds, shown in Fig. 4. The buckled triangular plane has a degree of freedom that is not present in either the flat triangular or the flat hexagonal plane. Buckling introduces a third dimension into the planar structure, enabling strain to be relaxed in an internal degree of freedom that does not break the planar symmetry. As the buckled plane is stretched, atoms can move perpendicular to the plane to relieve stress, an option that is forbidden by symmetry in flat planar structures. This is analogous to the fundamental difference between the phonon modes of a monatomic Bravais lattice and those of a lattice with a basis: in the latter, optical modes are present that allow relative motion without a net translation of the crystal. The larger $(4n,4n)$ boron nanotubes with buckled sides, such as the (8,8) tube, have unique mechanical properties that arise from the presence of these internal degrees of freedom. These nanotubes are not directly analogous to macroscopic tubes: longitudinal strain is not accompanied solely by an expansion or contraction of the tube radius, but rather by an additional relaxation of the tube structure. Controlling the chirality of boron nanotubes permits stress dissipation through novel internal mechanisms unique to nanoscale structures.

The enhanced lateral rigidity seen in (8,8) boron nanotubes could prove advantageous in the design of nanotube composite materials. Composites consisting of carbon nanotubes embedded in a polymer matrix have already been fabricated and result in a high-strength, lightweight material.[16–18] As Srivastava *et al.*[19] have pointed out, optimization of such a composite would require nanotubes with a high Young's modulus and a low Poisson ratio. The cylindrical symmetry of carbon nanotubes, only broken at high strains,[20] prevents them from reducing their Poisson ratio through internal relaxations as in (8,8) boron nanotubes. Composites using boron nanotubes could take advantage of the high Young's modulus of $(n,0)$ tubes to provide stiffness, while the low Poisson ratio of $(4n,4n)$ tubes could provide optimal stress transfer between the polymer matrix and the nanotubes. Boron nanotubes are the elastic analogue of carbon nanotubes: chirality dependence leads to tunable electrical properties in carbon tubes, and to tunable elastic properties in boron tubes. Just as the variation in electrical properties permits the design of carbon nanotube transistors,[22–24] boron nanotubes may find use in high-strength composites and nanoelectromechanical systems.[21]

In contrast to the $(n,n)$ nanotubes, the $(n,0)$ tubes have relatively low Poisson ratios. For example, the (8,0) tube has $\sigma=0.1$. Straining the tube stresses the nondirectional metallic bonds both laterally and longitudinally, since there is no dominant bonding direction. The stiffness of the metallic bonds, reflected in the high Young's moduli of the $(n,0)$ tubes, makes it difficult for the tube to expand or contract circumferentially. Unlike the $(n,n)$ tubes, structural dynamics do not seem to play a significant role in reducing the Young's modulus of the $(n,0)$ boron nanotubes.

In summary, we have investigated the unusual properties of planar and tubular boron structures. Although boron might be expected to form planar structures similar to carbon graphene sheets, a metallic triangular plane with a nearly homogeneous electron density has a larger cohesive energy. A threefold degenerate ground state in the flat plane makes it unstable with respect to buckling, which breaks the triangular symmetry and introduces a preferred direction. When the plane is rolled into a tube, this direction defines the chirality and controls the electronic and mechanical properties of the tube. $(n,n)$ boron nanotube structures are proposed that arise from the buckled plane and have lower curvature energies than the $(n,0)$ tubes arising from the flat triangular plane. As a result of buckling, $(n,n)$ boron nanotubes have an internal relaxation mechanism that results in a very low Poisson ratio. The electron density differences between the flat and buckled planes explains the differences in the elastic properties of the $(n,0)$ and $(n,n)$ tubes. Understanding planar boron structures is crucial to understanding the unusual properties of boron nanotubes.

This work was supported in part by the U.S. Department of Energy under Contract No. DE-FG02-99ER-45778, and by the William A. and Nancy F. McMinn Endowment at Vanderbilt University.

[1] A. E. Newkirk, in *Boron, Metallo-Boron Compounds, and Boranes*, edited by R. M. Adams (Wiley, New York, 1964).
[2] M. S. Dresselhaus, G. Dresselhaus, and P. C. Eklund, *Science of Fullerenes and Carbon Nanotubes* (Academic, San Diego, 1996).
[3] T. W. Ebbesen and P. M. Ajayan, Nature (London) **358**, 220 (1992); A. Thess, R. Lee, P. Nikolaev, H. Dai, P. Petit, J. Robert, C. Xu, Y. H. Lee, S. G. Kim, A. G. Rinzler, D. T. Colbert, G. E. Scuseria, D. Tománek, J. E. Fischer, and R. E. Smalley, Science **273**, 483 (1996).
[4] I. Boustani, A. Quandt, and A. Rubio, J. Solid State Chem. **154**, 269 (2000).
[5] I. Boustani, A. Quandt, E. Hernández, and A. Rubio, J. Chem. Phys. **110**, 3176 (1999).
[6] C. J. Otten, O. R. Lourie, M.-F. Yu, J. M. Cowley, M. J. Dyer, R. S. Ruoff, and W. E. Buhro, J. Am. Chem. Soc. **124**, 4564 (2002).
[7] L. Cao, J. Liu, C. Gao, Y. Li, X. Li, Y. Q. Wang, Z. Zhang, Q. Cui, G. Zou, L. Sun, and W. Wang, J. Phys.: Condens. Matter **14**, 11017 (2002); Y. Q. Wang and X. F. Duan, Chem. Phys. Lett. **367**, 495 (2003); X. M. Meng, J. Q. Hu, Y. Jiang, C. S. Lee, and S. T. Lee, Chem. Phys. Lett. **370**, 825 (2003).
[8] M. C. Payne, M. P. Teter, D. C. Allan, T. A. Arias, and J. D. Joannopoulos, Rev. Mod. Phys. **64**, 1045 (1992).
[9] X. Gonze, J.-M. Beuken, R. Caracas, F. Detraux, M. Fuchs, G.-M. Rignanese, L. Sindic, M. Verstraete, G. Zerah, F. Jollet, M. Torrent, A. Roy, M. Mikami, P. Ghosez, J.-Y. Raty, and D. C. Allan, Comput. Mater. Sci. **25**, 478 (2002).
[10] M. Fuchs and M. Scheffler, Comput. Phys. Commun. **119**, 67 (1999).
[11] J. Donohue, *The Structures of the Elements* (Wiley, New York, 1974), and references therein.
[12] N. Vast, S. Baroni, G. Zerah, J. M. Besson, A. Polian, M. Grimsditch, and J. C. Chervin, Phys. Rev. Lett. **78**, 693 (1997).
[13] J.-C. Charlier, X. Gonze, and J.-P. Michenaud, Phys. Rev. B **43**, 4579 (1991), and references therein.
[14] For details of the phonon calculation, see X. Gonze, Phys. Rev. B **55**, 10337 (1997).
[15] E. Hernández, C. Goze, P. Bernier, and A. Rubio, Phys. Rev. Lett. **80**, 4502 (1998).
[16] R. Andrews, D. Jacques, A. M. Rao, T. Rantell, F. Derbyshire, Y. Chen, J. Chen, and R. C. Haddon, Appl. Phys. Lett. **75**, 1329 (1999).
[17] E. T. Thostenson, Z. Ren, and T.-W. Chou, Compos. Sci. Technol. **61**, 1899 (2001).
[18] A. A. Mamedov, N. A. Kotov, M. Prato, D. M. Guldi, J. P. Wicksted, and A. Hirsch, Nat. Mater. **1**, 190 (2002).
[19] D. Srivastava, C. Wei, and K. Cho, Appl. Mech. Rev. **56**, 215 (2003).
[20] G. G. Samsonidze, G. G. Samsonidze, and B. I. Yakobson, Phys. Rev. Lett. **88**, 065501 (2002).
[21] H. G. Craighead, Science **290**, 1532 (2000).
[22] S. J. Tans, R. M. Verschueren, and C. Dekker, Nature (London) **393**, 49 (1998).
[23] P. Avouris, J. Appenzeller, R. Martel, and S. J. Wind, Proc. IEEE **91**, 1772 (2003).
[24] A. Javey, J. Guo, Q. Wang, M. Lundstrom, and H. Dai, Nature (London) **424**, 654 (2003).
[25] C. Kittel, *Introduction to Solid State Physics*, 2nd ed. (Wiley, New York, 1986), pp. 55–57.